Radiology

ORIGINAL RESEARCH • NEURORADIOLOGY

Resting-State Functional MRI of Healthy Adults: Temporal Dynamic Brain Coactivation Patterns

Tiantian Liu, BS • Li Wang, MD, PhD • Dingjie Suo, PhD • Jian Zhang, PhD • Kexin Wang, BS • Jue Wang, BS • Duanduan Chen, PhD • Tianyi Yan, PhD

From the School of Life Science (T.L., L.W., D.S., K.W., J.W., D.C., T.Y.) and Intelligent Robotics Institute, School of Mechatronical Engineering (J.Z.), Beijing Institute of Technology, 5 South Zhongguancun St, Haidian District, Beijing 100081, China. Received July 19, 2021; revision requested September 7; revision received January 24, 2022; accepted March 2. **Address correspondence to** T.Y. (email: yantianyi@bit.edu.cn).

Supported by the National Natural Science Foundation of China (grants U20A20191, 61727807, 82071912, and 12104049), Beijing Municipal Science & Technology Commission (grant Z201100007720009), Fundamental Research Funds for the Central Universities (grant 2021CX11011), and China Postdoctoral Science Foundation (grant 2020TQ0040). Cam-CAN funding was provided by the UK Biotechnology and Biological Sciences Research Council (grant number BB/H008217/1), together with support from the UK Medical Research Council and University of Cambridge, UK.

Conflicts of interest are listed at the end of this article

See also the editorial by Holodny in this issue.

Radiology 2022; 000:1–9 • https://doi.org/10.1148/radiol.211762 • Content codes: NR MR • © RSNA, 2022

Background: The aging brain is typically associated with aberrant interactions of large-scale intrinsic networks. However, the dynamic variation of these networks' coactivation or deactivation across the adult lifespan remains unclear.

Purpose: To promote the interpretation of dynamic brain network variations underlying the complex aging process by quantifying activation levels and obtaining a clear definition of coactivation patterns (CAPs) with resting-state functional MRI (rsfMRI).

Materials and Methods: In a retrospective study (October 2010 to September 2013), rsfMRI data from healthy participants in the Cambridge Centre for Ageing and Neuroscience (Cam-CAN) data repository were used to generate CAPs by applying single-volume temporal clustering analysis. Spatial clustering analysis was then performed to capture dynamic coactivation and deactivation within or between primary sensory networks and high-order cognitive networks (including the default mode network [DMN], attentional network [AN], and frontoparietal network [FPN]). Linear relationships between dynamic metrics and age were revealed with Spearman partial correlations.

Results: A total of 614 participants (mean age, 54 years ± 18 [SD]; 311 women) ranging in age from 18 to 88 years were evaluated. There was a negative correlation of the CAPs (Spearman correlations: $r = -0.98$, $P < .001$) with loss of coactivation (partial correlations: $r = -0.17$, $P < .001$) and deactivation (partial correlations: $r = 0.216$, $P < .001$) with aging. The CAPs, characterized by negative correlation patterns between the DMN and AN, occurred (partial correlations: $r = 0.14$, $P = .003$) and dwelled (partial correlations: $r = 0.10$, $P = .04$) more with aging. Moreover, the AN and DMN CAP transitioned more to the AN and FPN CAP with aging (partial correlations: $r = 0.17$, $P < .001$).

Conclusion: The dynamics of the healthy aging brain are characterized mainly by more flexibility of the high-order cognitive networks while maintaining primary sensory functions (networks).

Online supplemental material is available for this article.

Previous resting-state functional MRI (rsfMRI) studies have consistently indicated that young and old healthy individuals display different intrinsic functional connectivity patterns (1), a difference that may mediate the negative impacts of aging on cognitive function (2). Intrinsic networks are highly segmented to support specialized cognitive processes. The primary sensory network (PSN) plays a critical role in primary information processing, while networks such as the attentional network (AN), frontoparietal network (FPN), default mode network (DMN), and limbic network play a critical role in high-order cognitive control functions. Aging-related intrinsic network alterations show a mirroring pattern with network development, which is called the "last-in, first-out" theory. This theory posits that brain development shifts from the PSN to high-order cognitive control networks (3), but healthy aging begins with high-order cognitive networks and maintains relatively intact primary functions (4). The "last-in, first-out" theory holds that the PSN and high-order cognitive networks show disparate changes with aging (5).

In addition to segregation, intrinsic networks are extremely integrated to cooperate or compete during concrete cognitive control tasks. A representative integration is the negative correlation between the DMN and AN (6,7). To perform better during the goal-directed tasks, the brain may assemble the DMN and AN to complete the competitive processes between external goal-directed attention and internal mindful processes (6). A study on aging has shown a small magnitude of DMN-AN negative correlations, which may induce the dysfunctions of working memory (8). In addition, the FPN, a critical switch node of cognitive control, is thought to be able to modulate interactions between the DMN and AN with an age-sensitive feature (9,10). This raises the question on how the network

Abbreviations

AN = attentional network, Cam-CAN = Cambridge Centre for Ageing and Neuroscience, CAP = coactivation pattern, DMN = default mode network, FPN = frontoparietal network, PSN = primary sensory network, ROI = region of interest, rsfMRI = resting-state functional MRI

Summary

Temporal dynamic changes of the aging brain with resting-state functional MRI demonstrated lower flexibility of the frontoparietal network and compensatory higher transitions between the default mode and the attentional network.

Key Results

- In a retrospective study using the Cambridge Centre for Ageing and Neuroscience repository data from 614 healthy individuals (age: 18–88 years), adults spent more time in the resting-state attentional network (AN) and default mode network (DMN) coactivation pattern (CAP) at functional MRI with aging (partial correlations: $r = 0.14$, $P = .003$).
- The AN and DMN CAP transitioned to an AN and frontoparietal network CAP with aging (partial correlations: $r = 0.17$, $P < .001$).
- Primary sensory functions (networks) are relatively maintained in healthy aging.

interactions among the DMN, AN, and FPN temporally change across the adult lifespan.

Researchers have characterized three (11) and five (12) aging-related brain states within specific sliding windows. Compared with sliding-window analyses, coactivation pattern (CAP) analysis has identified recurrent patterns of spontaneous brain activity at frame resolution (13). The findings indicate that a limited number of spatially reproducible and temporally recurring dominant CAPs can explain spontaneous spatiotemporal dynamics to a great degree. Therefore, we applied spatial clustering to traditional CAP analysis (14) and characterized dynamic variations of large-scale function networks with aging.

The purpose of this study was to promote the interpretation of dynamic brain network variations underlying the complex aging process by quantifying activation levels and obtaining a clear definition of CAPs with rsfMRI.

Materials and Methods

Study Sample

The retrospective study (October 2010 to September 2013) sample was drawn from the Cambridge Centre for Ageing and Neuroscience (Cam-CAN) repository (available at *http://www.mrc-cbu.cam.ac.uk/datasets/camcan/*) (15,16) (Fig 1). All participants gave written informed consent. According to the Declaration of Helsinki, the Cambridgeshire 2 Research Ethics Committee approved the project. The exclusion criteria are listed in Appendix E1 (online).

Imaging Protocol

The structural (repetition time msec/echo time msec, 2250/2.99) and functional (1970/30) MRI data were obtained with a MAGNETOM Trio, A Tim System 3T eco (Siemens Healthineers) with a 32-channel head coil. rsfMRI time lasted

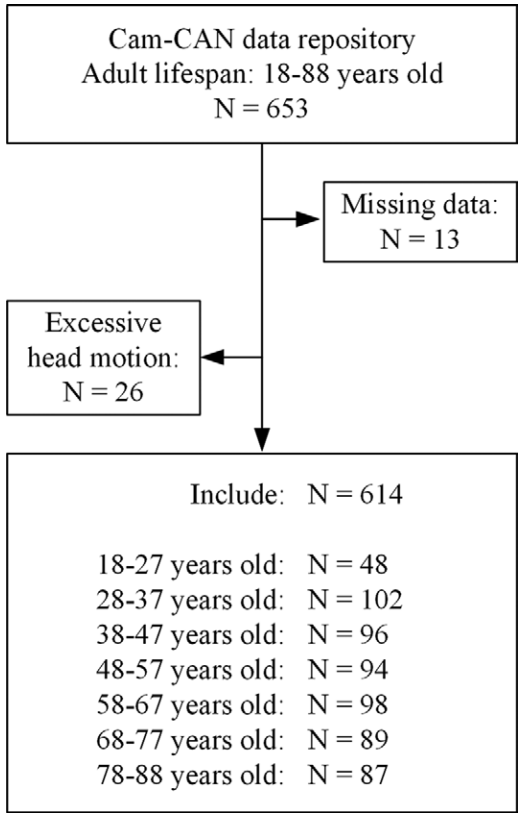

Figure 1: Flowchart of participants. A total of 614 participants from the Cambridge Centre for Ageing and Neuroscience (Cam-CAN) repository were included in the study.

for 8 minutes 40 seconds, including a total of 261 volumes. More details are provided in the Cam-CAN publications (15,16) and in Appendix E2 (online).

Data Preprocessing

rsfMRI data were preprocessed by using Statistical Parametric Mapping 12 *(https://www.fil.ion.ucl.ac.uk/spm/)* and the Data Processing & Analysis of Brain Imaging 3.1 tool (17) in MATLAB 2014a (MathWorks) (K.W. and J.W., both with 5 years of experience). The first 10 volumes of rsfMRI data were discarded. Images then underwent section timing correction (reference section: middle section), head motion correction, band-pass filtering (range, 0.01–0.1 Hz), coregistration, and segmentation. Then, images were spatially normalized into the Montreal Neurological Institute space and smoothed with a Gaussian filter (full width at half maximum: 4 mm). Global mean signal intensity, white matter signal intensity, cerebrospinal fluid signal intensity, and global Friston 12-motion parameters (six motion parameters and six motion derivatives) were regressed out as nuisance covariates.

Region of Interest–wise CAP Construction

As shown in Figure 2, we used high-spatial-resolution brain parcellation with 1024 regions of interest (ROIs) (18) to perform whole-brain ROI-wise CAP analysis. A total of 154 114 volumes (614 participants multiplied by 251 volumes) and 1024 features were temporally clustered based on their spatial dissimilarity. *k*-means clustering was replicated 500 times with *k* ranging from

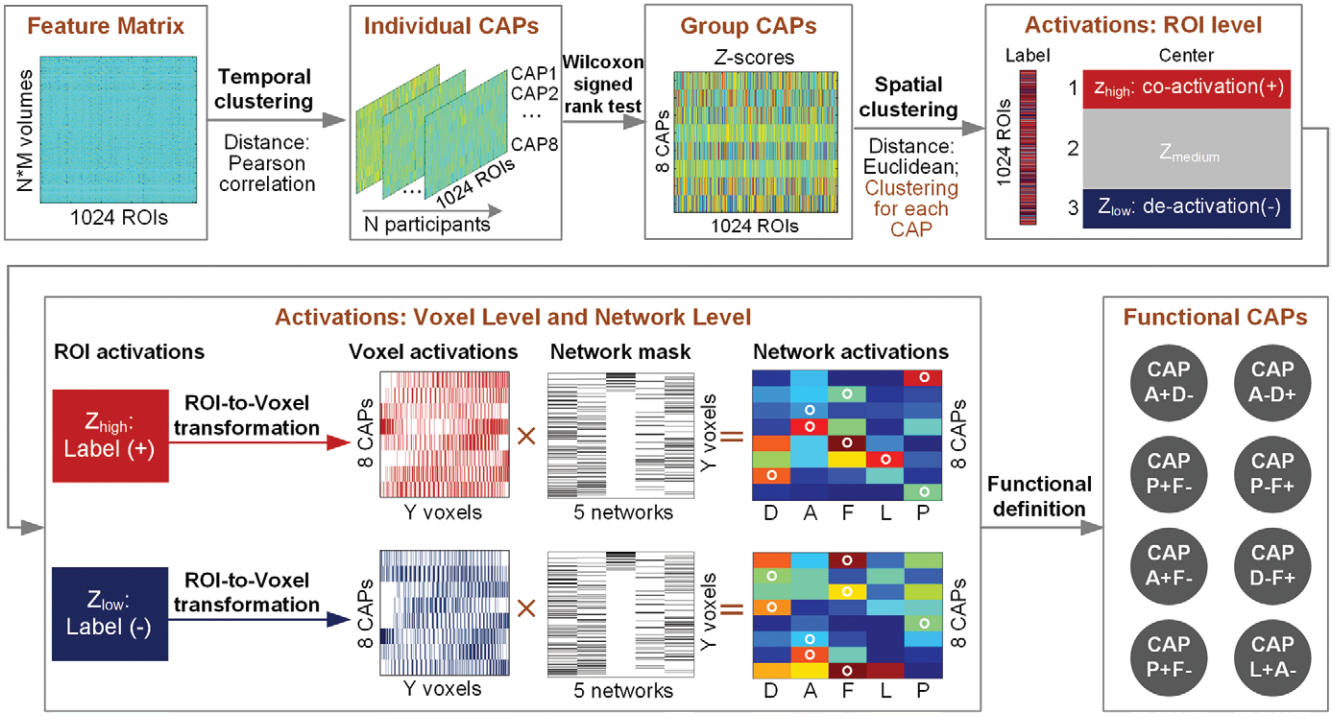

Figure 2: Outline of the coactivation pattern (CAP) analysis. Preprocessed images were parcellated into 1024 regions of interest (ROIs). The average signals in each ROI were calculated as features. Thus, the feature matrix (total: $N \times M$ volumes and 1024 ROIs, where N = number of participants, M = volumes of each participant) was evaluated with temporal clustering analysis. Clustering analysis was performed to maximize the distance between clusters and minimize the distance within clusters. After temporal clustering analysis, we obtained the label of each volume. Volumes with the same labels were temporally averaged for each participant to obtain individual CAPs. A Wilcoxon signed-rank test was performed for all participants, and group CAPs were obtained. The *z* scores of each CAP (group CAPs: 1024 ROIs and the *z* score) were evaluated by means of spatial clustering analysis with Euclidean distance. After spatial clustering analysis, we obtained the label of each ROI and defined ROI-level coactivations or deactivations according to the center defined in the clustering analysis. In detail, ROIs labeled with higher *z* scores (Z_{high}) showed coactivations, and ROIs labeled with lower *z*-scores (Z_{low}) showed deactivations. The previously mentioned ROI-level activations were transformed to the voxel level and then multiplied by the network mask. The resulting peak network-level activations are marked with white circles in the matrix of network activations. Finally, functional CAPs were defined by the previously mentioned peak network activations. The five networks were as follows: attentional network (A), default mode network (D), frontoparietal network (F), limbic network (L), and primary sensory network (P). The "+" symbol indicates coactivation, and the "−" symbol indicates deactivation.

2 to 10. Volumes with the same label were then averaged to produce *k* overall CAPs of all the participants. The volumes for each participant were averaged to produce *k* individual CAPs based on individual time series. Additional details are provided in Appendix E3 (online).

ROI-wise CAP Definition

Spatial clustering analysis was applied to the *z* scores of each CAP to identify relatively larger coactivations and deactivations. In detail, a vector with 1024 *z* scores corresponding to one CAP was evaluated by spatial clustering analysis, and the distance was Euclidean. *k*-means clustering was replicated 500 times (for $k = 3$) to reveal high-level, medium-level, and low-level activations. We then defined the functional CAPs according to the peak ratio.

Global and Local Metrics of CAPs

Global amplitude and variability were calculated with the mean and SD values of ROI signals in individual CAPs. We then parcellated 1024 ROIs into five networks (the PSN, AN, FPN, DMN, and limbic network) according to a previous template (19). The mean signal in each network was calculated for each CAP as local activations of CAPs.

Temporal Analysis of Aging-related CAPs

After clustering analysis, the dynamics of each participant were described with a vector of labels that varied from 1 to *k*. The vector suggests that the participant exhibited different CAPs at different time points. Occurrence was defined based on the vector as the proportion of the specific label found in this vector. The dwell time was defined as the time during which the same label was assigned consecutively in the vector. The occurrence and dwell time were calculated to characterize temporal changes with aging. In addition to occurrence and dwell time, transition times characterized the transfer probability between CAPs. The transition time between two CAPs was defined as the number of transfers between different labels.

Statistical Analysis

Generalized estimating equation analysis was performed in SPSS (version 23.0, IBM SPSS Statistics) and other statistical analysis was performed in MATLAB 2014a (MathWorks) (T.L. and J.Z., with 7 and 13 years of experience, respectively). Wilcoxon signed-rank tests were used to evaluate whether the median of ROI-wise signals differed from zero. Spearman correlations were used to evaluate similarities among CAPs.

Each participant had one value of mean framewise displacement, amplitude, variability, occurrence, and dwell time for each CAP. Generalized estimating equation and post hoc analyses were used to evaluate the differences of the previously mentioned variables between CAPs. Linear relationships between age and metrics were estimated by using Spearman partial correlations (ie, amplitude, variability, local activations, occurrence, dwell time, and transition time) (11,20). Sex, mean framewise displacement (21), number of framewise displacements greater than 0.5 mm, and gray matter volume (17) were regarded as covariates. False discovery rate–corrected $P < .05$ was considered statistically significant. When statistically significant partial correlations between age and specific metrics were found, the metrics underwent further Spearman partial correlations with the total fluid intelligence score (15), with the same covariates as mentioned previously. Additional details are provided in Appendix E4 (online).

Results

Characteristics of Study Sample

The total number of participants in the Cam-CAN study was 653; this included 13 participants with missing data and 26 with excessive head motion (head movements were larger than 3 mm or 3°). Finally, 614 participants (mean age ± SD: 54 years ± 18; age range: 18–88 years; 311 women; mean fluid intelligence score: 32.0 points ± 6.6) were evaluated (Fig 1, Table).

Functional CAPs

The results of clustering analysis showed that the eight-cluster solution yielded high similarities within CAPs and high differences among CAPs (Fig E1 [online]). The eight CAPs resulting from the temporal clustering analysis showed different head motion levels. Generalized estimating equation and post hoc pairwise comparisons showed that the framewise displacement values of two CAPs, CAP 6 (mean, 0.18 ± 0.10) and CAP 8 (mean, 0.17 ± 0.10), were larger (all *P* values are shown in Table E1 [online]) than those of other CAPs (CAP 1, 0.15 ± 0.09; CAP 2, 0.15 ± 0.08; CAP 3, 0.16 ± 0.08; CAP 4, 0.15 ± 0.07; CAP 5, 0.15 ± 0.07; CAP 7, 0.14 ± 0.07), suggesting that CAP 6 and CAP 8 were highly affected by head motion. As was performed in a previous study (22), those two CAPs were removed, and the subsequent analysis focused on the other six CAPs.

Six functional CAPs (CAP A+D–, CAP A–D+, CAP P+F–, CAP P–F+, CAP A+F–, and CAP D–F+; where A indicates AN, D indicates DMN, P indicates PSN, and F indicates FPN) were defined according to the peak coactivations (indicated with a plus sign) (Fig 3A) and deactivations (indicated with a minus sign) (Fig 3B) observed in each network. Five-network parcellation is shown in Figure 4B. CAP 7 showed a high ratio of coactivations in the DMN (ratio = 0.70) and deactivations in the AN (ratio = 0.70), while CAP 4 showed a high ratio of coactivations in the AN (ratio = 0.75) and deactivations in the DMN (ratio = 0.65). CAP 5 showed a high ratio of coactivations in the FPN (ratio = 0.86) and deactivations in the PSN (ratio = 0.43), while CAP 1 showed a high ratio of coactivations in the PSN (ratio = 0.81) and deactivations in the FPN (ratio = 0.86).

Z scores obtained with the Wilcoxon signed-rank test for each CAP are shown in Figure 4A. We found a total of three pairs of CAPs with high dissimilarities (all Spearman *r* values are shown in Fig E2 [online]). The first CAP pair showed anticorrelated patterns of AN and DMN coactivations ($r = -0.98$, $P < .001$). The second pair showed anticorrelated patterns of PSN and FPN coactivations ($r = -0.97$, $P < .001$). The third pair showed anticorrelated patterns of AN and limbic network and FPN coactivations ($r = -0.81$, $P < .001$).

Global and Local Metrics of CAPs

As shown in Figure E3 (online), CAP P+F– showed the maximum amplitude (mean, 0.48 ± 0.23), while CAP A+F– showed the minimum amplitude (mean, 0.39 ± 0.19; $P < .001$). Both of the previously mentioned CAPs were correlated with age (CAP P+F–: $r = -0.15$, $P < .001$; CAP A+F–: $r = -0.09$, $P = .03$) but not with fluid intelligence (CAP P+F–: $r = 0.02$, $P = .69$; CAP A+F–: $r = 0.03$, $P = .61$). CAP P–F+ showed the highest variability (mean, 0.42 ± 0.21) and was correlated with age ($r = -0.13$, $P = .003$), while CAP A+F– showed the lowest variability (mean, 0.36 ± 0.18; $P < .001$, compared with CAP P–F+) and was not correlated with age ($r = -0.04$, $P = .28$). Additional details are provided in Tables E2 and E3 (online).

In addition, the local metric, DMN activations of CAP A+D–, was positively correlated with age ($r = 0.20$, $P < .001$) and negatively correlated with fluid intelligence ($r = -0.13$, $P = .02$). DMN deactivations of CAP A–D+ correlated negatively with age ($r = -0.16$, $P < .001$) but did not correlate with fluid intelligence ($r = 0.07$, $P = .13$). Other partial correlations with age were found in AN (CAP A+D–: $r = -0.17$, $P < .001$; CAP A–D+: $r = 0.13$, $P = .002$), FPN (CAP A+F–: $r = 0.14$, $P < .001$; CAP P+F–: $r = 0.17$, $P < .001$; CAP P–F+: $r = -0.12$, $P = .003$; CAP D–F+: $r = -0.14$, $P < .001$), and PSN (CAP P+F–: $r = -0.20$, $P < .001$; CAP P–F+: $r = -0.18$, $P < .001$). Additional details are provided in Tables E4 and E5 (online).

Temporal Characteristics of Aging-related CAPs

As shown in Figure 5, CAP P+F– showed the maximum occurrence (mean, 0.14 ± 0.13), while CAP D–F+ showed the minimum occurrence (mean, 0.10 ± 0.08; $P < .001$). CAP P–F+ showed the maximum dwell time (mean, 6.03 time points ± 10.58), while CAP D–F+ showed the minimum dwell time (mean, 4.67 time points ± 8.71; $P < .001$). In addition, the occurrence of three CAPs correlated with age (CAP A–D+: $r = 0.14$, $P = .003$; CAP A+D–: $r = 0.12$, $P = .01$; CAP P–F+: $r = -0.15$, $P = .003$) and fluid intelligence (CAP A–D+: $r = -0.09$, $P = .04$; CAP A+D–: $r = -0.10$, $P = .03$; CAP P–F+: $r = 0.13$, $P = .008$). The dwell time of CAP A–D+ correlated with age ($r = 0.10$, $P = .04$) but not with fluid intelligence ($r = -0.05$, $P = .25$). Additional details are shown in Figure E4 and Table E6 (online).

All transition times are shown in the transition matrix (Fig 6A). According to the transition matrix, CAP A–D+

Participant Demographics per Age Decile

Characteristic	Decile 1	Decile 2	Decile 3	Decile 4	Decile 5	Decile 6	Decile 7
Age range (y)	18–27	28–37	38–47	48–57	58–67	68–77	78–88
No. of participants	48	102	96	94	98	89	87
Sex							
M	22	49	47	46	49	48	42
F	26	53	49	48	49	41	45
Fluid intelligence (points)*	37.7 ± 3.4	37.1 ± 4.3	35.2 ± 4.3	33.6 ± 4.5	30.5 ± 5.3	27.5 ± 5.8	24.2 ± 5.6

Note.—The number of participants older than 65 years is 206.
* Data are means ± SDs.

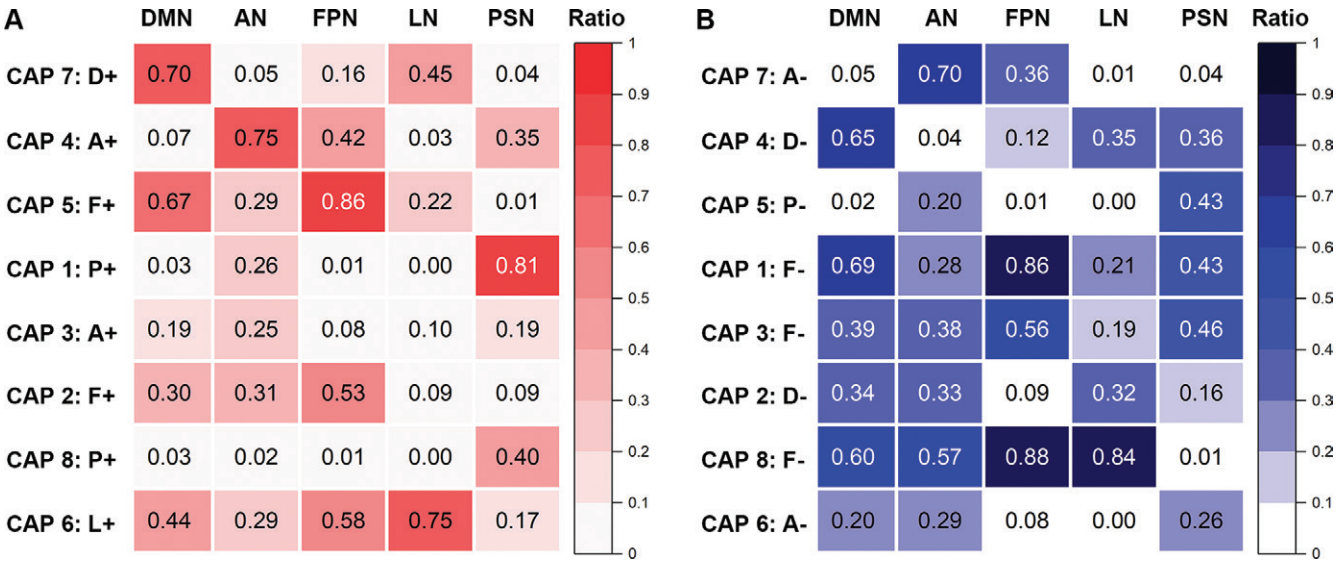

Figure 3: Ratio of peak activations in each network for different coactivation patterns (CAPs). **(A)** Matrix shows average coactivations (relatively higher positive *z* scores in the spatial clustering analysis) in each network. **(B)** Matrix shows average deactivations (relatively higher negative *z* scores in the spatial clustering analysis) in each network. Each element in the matrix indicates the ratio of peak coactivation and deactivation voxels to all voxels in the network. The peak ratio in each row is marked with the name of the CAP. For example, "CAP 1: P+" indicates that the first CAP showed peak coactivations in the primary sensory network. "A" or "AN" indicates attentional network, "D" or "DMN" indicates default mode network, "F" or "FPN" indicates frontoparietal network, "L" or "LN" indicates limbic network, and "P" or "PSN" indicates primary sensory network. The "+" symbol indicates coactivation, and the "−" symbol indicates deactivation.

maximally transfers to itself (11 085 times) and minimally transfers to CAP A+D– (205 times). This observation suggested that each CAP was most easily transferred to itself and least easily transferred to the anticorrelated CAP. In addition, three transitions correlated positively with age, including transitions from CAP A–D+ to CAP A–D+ ($r = 0.14$, $P < .001$), from CAP A+D– to CAP A+D– ($r = 0.15$, $P < .001$), and from CAP A+D– to CAP A+F– ($r = 0.17$, $P < .001$) (Figs 6B, E5 [online]). One of these transitions, the transition from CAP A+D– to CAP A+F–, correlated negatively with fluid intelligence ($r = -0.11$, $P = .01$) (Fig 6C).

Discussion

To further clarify variations of coactivation or deactivation of large-scale intrinsic networks across the adult lifespan, we carried out this retrospective study to measure changes in coactivation patterns (CAPs) by using resting-state functional MRI data from 614 healthy individuals with a wide age range of 18–88 years in the Cambridge Centre for Ageing and Neuroscience repository to promote the interpretation of dynamic brain network variations. In addition to the anticorrelated CAPs between attentional network (AN) and default mode network (DMN) ($r = -0.98$, $P < .001$), similar to what was previously found in negative correlations between these two networks (6), we also found anticorrelated CAPs between primary sensory and frontoparietal networks ($r = -0.97$, $P < .001$). After correlation analyses, we found that the AN and DMN CAPs occurred ($r = 0.14$, $P = .003$) and transitioned ($r = 0.17$, $P < .001$) more with aging, indicating that these two networks are key components of age-related changes by serving as a compensatory increased response to cognitive decline.

Although static functional connectivity has been shown to be nonlinearly correlated with aging (3), temporal changes of dynamic functional connectivity and brain states are considered to correlate linearly with aging (11,20). In this study, linear correlation

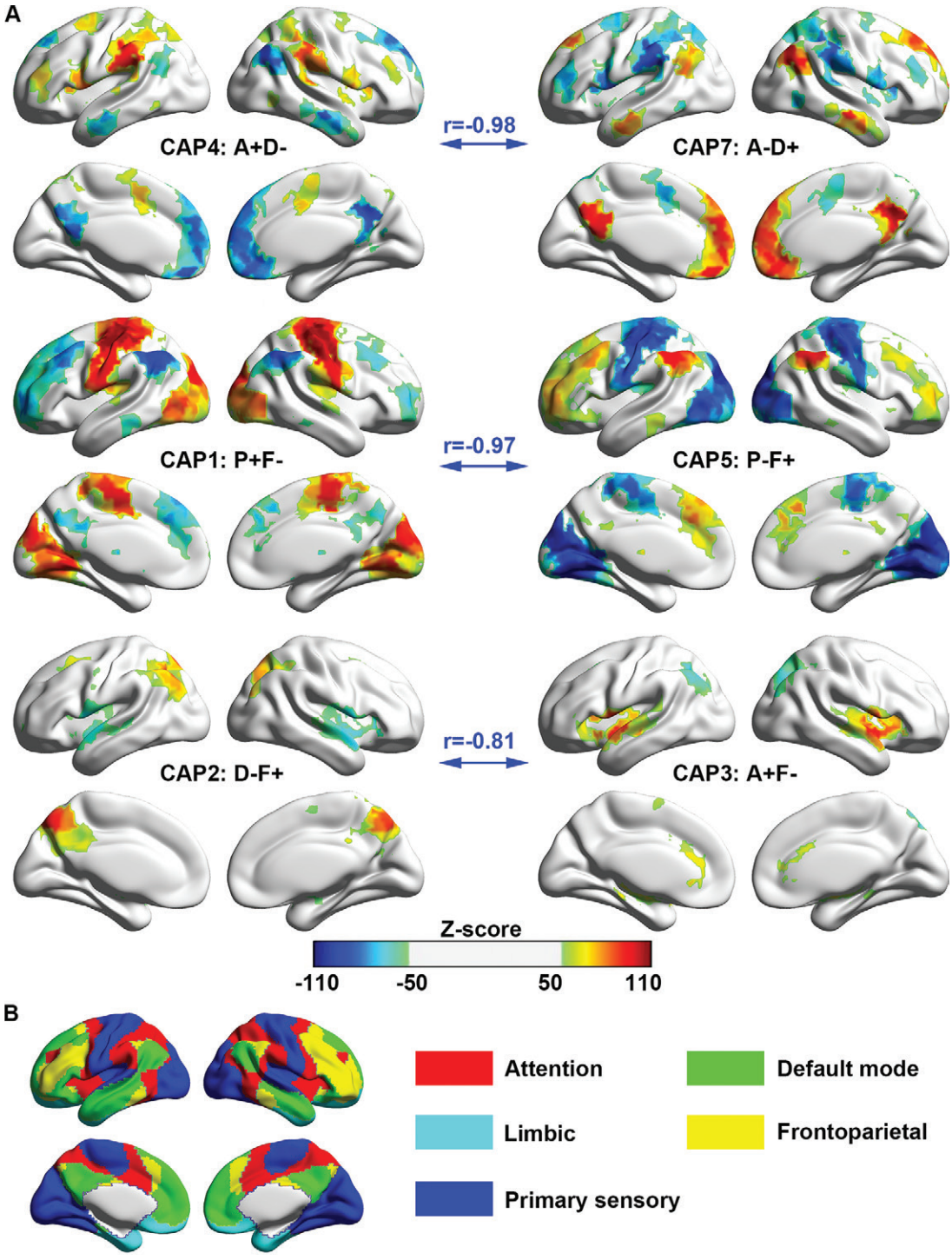

Figure 4: Group functional coactivation patterns (CAPs). **(A)** *Z* scores of six CAPs. Each row shows one pair of CAPs, and the Spearman correlation *r* values are shown in the middle. A = attentional network, D = default mode network, F = frontoparietal network, P = primary sensory network. The "+" symbol indicates coactivation, and the "−" symbol indicates deactivation. **(B)** Five-network template of 1024 regions of interest derived from a previous publication (19).

analysis showed that the PSN and FPN CAP occurred less with aging, while the AN and DMN CAP occurred more. Older adults (those older than 65 years) have shown reduced interactions between the FPN and DMN (10), which may result in less occurrence of FPN. The explanation for aging-related underactivation has always been that it is a mark of impairment due to structural changes such as atrophy, while aging-related overactivation is compensatory (23). More occurrences of the DMN and AN CAP can be considered as compensation to the PSN and FPN CAP. In addition, the FPN can flexibly change its network patterns with task demands (24), interacting more with the DMN at rest and with the AN in the multisource interference task state (10). Although

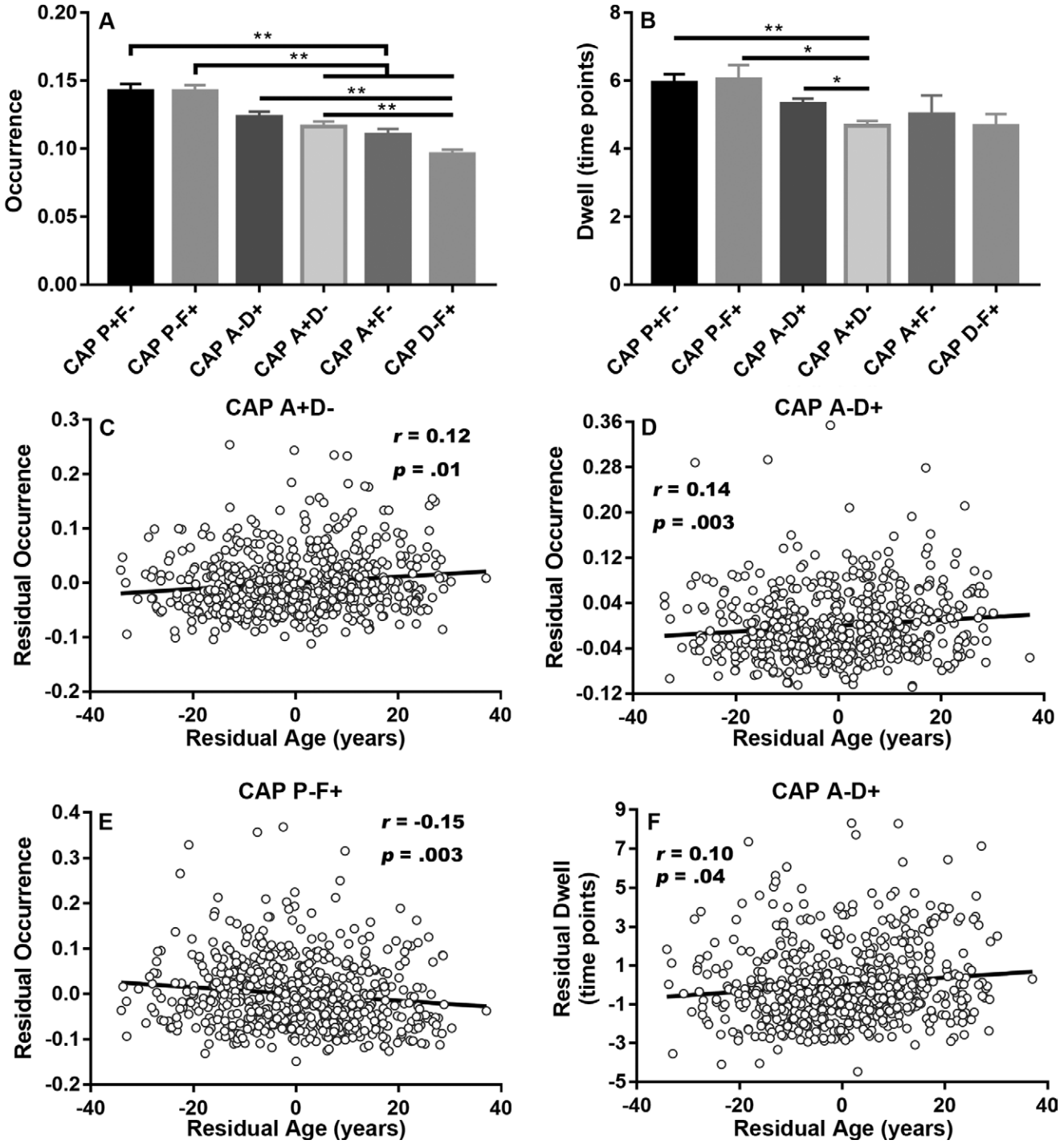

Figure 5: Temporal metrics. **(A, B)** Bar graphs show differences in **(A)** occurrence and **(B)** dwell time between coactivation patterns (CAPs). Generalized estimating equation and post hoc analyses were used to evaluate differences of each pair of CAPs. Mean and standard error of mean values are shown in each bar. * = Bonferroni-corrected $P < .05$ between two CAPs, ** = Bonferroni-corrected $P < .01$. **(C–F)** Scatterplots show partial correlation between residual age and **(C)** the occurrence of CAP A+D−, **(D)** the occurrence of CAP A−D+, **(E)** the occurrence of CAP P−F+, and **(F)** the dwell time of CAP A−D+. The correlation coefficient *P* values are corrected by false discovery rate for multiple comparisons. A = attentional network, D = default mode network, F = frontoparietal network, P = primary sensory network. The "+" symbol indicates coactivation, and the "−" symbol indicates deactivation.

negative correlations between the FPN and PSN have not yet been reported, a magnetoencephalography study has shown top-down modulation of the FPN on the primary sensory cortex (25). This motivates the application of high-temporal-resolution neuroimaging to clarify the mechanism of the negative correlations.

From the dynamic network perspective, we found that the DMN and AN CAP transitioned more with aging, but the PSN and FPN CAP showed no correlation with age, indicating that relatively intact primary sensory functions are maintained in healthy aging (4). This is supported by the

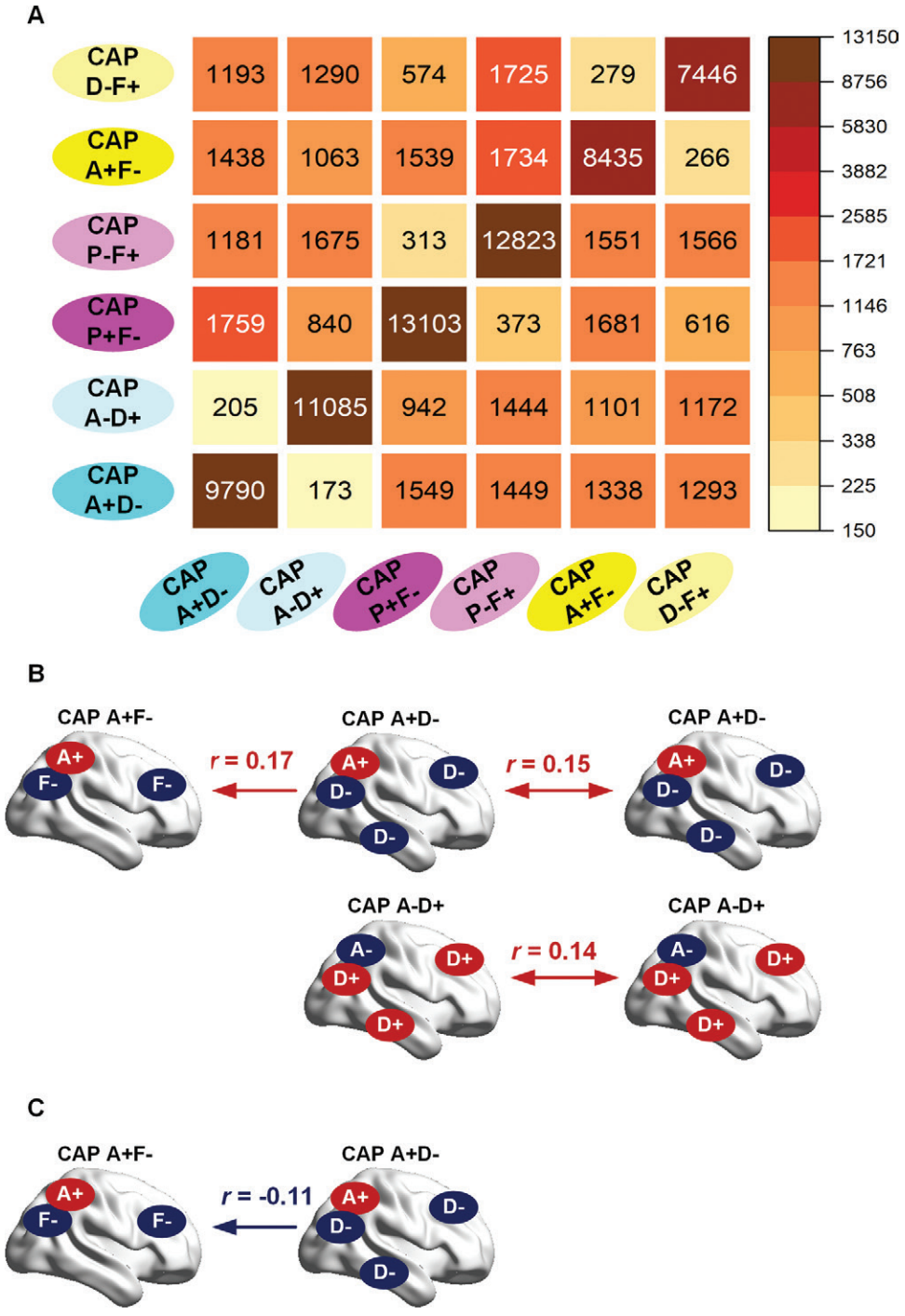

Figure 6: **(A)** Transition matrix among different coactivation patterns (CAPs). The elements in the matrix indicate the transition times from the corresponding row CAP to the corresponding column CAP. **(B)** Correlations between transitions and participant age. **(C)** Correlations between transitions and fluid intelligence. Only significant correlations are shown ($P < .05$, Bonferroni corrected for multiple comparisons). Positive correlations in **B** and **C** are indicated by red, and negative correlations are indicated by blue. Single arrows indicate the direction of transition, and double arrows indicate a reciprocal transfer. Partial correlation *r* values are shown next to the arrows. A = attentional network, D = default mode network, F = frontoparietal network, P = primary sensory network. The "+" symbol indicates coactivation, and the "−" symbol indicates deactivation.

"last-in, first-out" theory, which posits that during brain aging there is a shift from high-order cognitive networks to the PSN (3), and the DMN and AN are key networks affected by aging (2,9,26,27). These findings suggest neural strategies to maintain normal information transfer between brain regions in the presence of structural and microscopic changes in the aging brain (28).

Finally, we found that strong dominance of the DMN and AN CAP was negatively correlated with fluid intelligence in adults aged 18–88 years. In young adults (approximately 20–35 years old), the stronger anticorrelation between the DMN and AN has been linked to better cognitive performance (29). Our results showed that strong dominance of the DMN and AN CAP was correlated with poor cognitive performance, indicating inefficient cognitive strategies. The inefficient compensatory mechanism is also supported by the pathologic aging study of amnestic mild cognitive impairment, a prodromal phase of Alzheimer disease. Individuals with amnestic mild cognitive impairment have exhibited poorer cognitive function but greater negative correlation between DMN and AN (30).

Several limitations of this study should be mentioned. First, the optimal number of CAPs is not clear; this limitation also applies to *k*-means clustering analysis conducted with sliding windows (11). Hence, we used silhouette coefficients to maximize similarities within individual CAPs. Second, the hemodynamic response determines the measurable time interval (usually 1–2 seconds) between time points. This means that mixed but not distinct CAPs will be observed if neuronal events are shorter than the measurable time interval (14). Third, brain volume and blood oxygen level–dependent signals change with aging, and this may influence the explanation of CAPs. Thus, we used gray matter volume as a covariate and calculated the amplitude (mean blood oxygen level–dependent signal) of CAPs to partially reveal the signal differences.

In conclusion, our study characterizes aging-related large-scale network changes based on resting-state functional MRI data with use of coactivation pattern (CAP) analysis, a method that provides high temporal resolution close to a single functional MRI volume. Results suggest that adults spend less time in the primary sensory network and frontoparietal network CAP with aging, further leading to a compensatory larger occurrence of the default mode network and attentional network CAP. These findings provide insights into framewise aging-related network patterns and identify patterns that can serve as markers of brain disease and treatment targets of individualized neuromodulation, such as real-time functional MRI neurofeedback (31).

Acknowledgments: The authors thank Kewei Chen, PhD, for his suggestions on statistical analysis. Data collection and sharing for this project was provided by the Cambridge Centre for Ageing and Neuroscience (Cam-CAN).

Author contributions: Guarantors of integrity of entire study, **D.S., K.W., J.W., T.Y.**; study concepts/study design or data acquisition or data analysis/interpretation, all authors; manuscript drafting or manuscript revision for important intellectual content, all authors; approval of final version of submitted manuscript, all authors; agrees to ensure any questions related to the work are appropriately resolved, all authors; literature research, **T.L., D.S., K.W., J.W.**; clinical studies, **T.L., D.S., J.W.**; statistical analysis, **T.L., D.S., J.W., T.Y.**; and manuscript editing, **T.L., L.W., D.S., J.W., D.C.**

Disclosures of conflicts of interest: **T.L.** No relevant relationships. **L.W.** No relevant relationships. **D.S.** No relevant relationships. **J.Z.** No relevant relationships. **K.W.** No relevant relationships. **J.W.** No relevant relationships. **D.C.** No relevant relationships. **T.Y.** No relevant relationships.

References

1. Ferreira LK, Busatto GF. Resting-state functional connectivity in normal brain aging. Neurosci Biobehav Rev 2013;37(3):384–400.
2. Hughes C, Faskowitz J, Cassidy BS, Sporns O, Krendl AC. Aging relates to a disproportionately weaker functional architecture of brain networks during rest and task states. Neuroimage 2020;209:116521.
3. Edde M, Leroux G, Altena E, Chanraud S. Functional brain connectivity changes across the human life span: From fetal development to old age. J Neurosci Res 2021;99(1):236–262.
4. Naik S, Banerjee A, Bapi RS, Deco G, Roy D. Metastability in Senescence. Trends Cogn Sci 2017;21(7):509–521.
5. Geerligs L, Renken RJ, Saliasi E, Maurits NM, Lorist MM. A Brain-Wide Study of Age-Related Changes in Functional Connectivity. Cereb Cortex 2015;25(7):1987–1999.
6. Fox MD, Snyder AZ, Vincent JL, Corbetta M, Van Essen DC, Raichle ME. The human brain is intrinsically organized into dynamic, anticorrelated functional networks. Proc Natl Acad Sci U S A 2005;102(27):9673–9678.
7. Doucet G, Naveau M, Petit L, et al. Brain activity at rest: a multiscale hierarchical functional organization. J Neurophysiol 2011;105(6):2753–2763.
8. Keller JB, Hedden T, Thompson TW, Anteraper SA, Gabrieli JDE, Whitfield-Gabrieli S. Resting-state anticorrelations between medial and lateral prefrontal cortex: association with working memory, aging, and individual differences. Cortex 2015;64:271–280.
9. Grady C, Sarraf S, Saverino C, Campbell K. Age differences in the functional interactions among the default, frontoparietal control, and dorsal attention networks. Neurobiol Aging 2016;41:159–172.
10. Avelar-Pereira B, Bäckman L, Wåhlin A, Nyberg L, Salami A. Age-Related Differences in Dynamic Interactions Among Default Mode, Frontoparietal Control, and Dorsal Attention Networks during Resting-State and Interference Resolution. Front Aging Neurosci 2017;9:152.
11. Tian L, Li Q, Wang C, Yu J. Changes in dynamic functional connections with aging. Neuroimage 2018;172:31–39.
12. Xia Y, Chen Q, Shi L, et al. Tracking the dynamic functional connectivity structure of the human brain across the adult lifespan. Hum Brain Mapp 2019;40(3):717–728.
13. Zhang J, Huang Z, Tumati S, Northoff G. Rest-task modulation of fMRI-derived global signal topography is mediated by transient coactivation patterns. PLoS Biol 2020;18(7):e3000733.
14. Liu X, Zhang N, Chang C, Duyn JH. Co-activation patterns in resting-state fMRI signals. Neuroimage 2018;180(Pt B):485–494.
15. Taylor JR, Williams N, Cusack R, et al. The Cambridge Centre for Ageing and Neuroscience (Cam-CAN) data repository: Structural and functional MRI, MEG, and cognitive data from a cross-sectional adult lifespan sample. Neuroimage 2017;144(Pt B):262–269.
16. Shafto MA, Tyler LK, Dixon M, et al. The Cambridge Centre for Ageing and Neuroscience (Cam-CAN) study protocol: a cross-sectional, lifespan, multidisciplinary examination of healthy cognitive ageing. BMC Neurol 2014;14(1):204.
17. Yan CG, Wang XD, Zuo XN, Zang YF. DPABI: Data Processing & Analysis for (Resting-State) Brain Imaging. Neuroinformatics 2016;14(3):339–351.
18. Zalesky A, Fornito A, Harding IH, et al. Whole-brain anatomical networks: does the choice of nodes matter? Neuroimage 2010;50(3):970–983.
19. Yeo BTT, Krienen FM, Sepulcre J, et al. The organization of the human cerebral cortex estimated by intrinsic functional connectivity. J Neurophysiol 2011;106(3):1125–1165.
20. Zhang H, Lee A, Qiu A. A posterior-to-anterior shift of brain functional dynamics in aging. Brain Struct Funct 2017;222(8):3665–3676.
21. Jenkinson M, Bannister P, Brady M, Smith S. Improved optimization for the robust and accurate linear registration and motion correction of brain images. Neuroimage 2002;17(2):825–841.
22. Kaiser RH, Kang MS, Lew Y, et al. Abnormal frontoinsular-default network dynamics in adolescent depression and rumination: a preliminary resting-state co-activation pattern analysis. Neuropsychopharmacology 2019;44(9):1604–1612.
23. Cabeza R, Albert M, Belleville S, et al. Maintenance, reserve and compensation: the cognitive neuroscience of healthy ageing. Nat Rev Neurosci 2018;19(11):701–710 [Published correction appears in Nat Rev Neurosci 2018;19(12):772.].
24. Cole MW, Reynolds JR, Power JD, Repovs G, Anticevic A, Braver TS. Multi-task connectivity reveals flexible hubs for adaptive task control. Nat Neurosci 2013;16(9):1348–1355.
25. Wallis G, Stokes M, Cousijn H, Woolrich M, Nobre AC. Frontoparietal and Cingulo-opercular Networks Play Dissociable Roles in Control of Working Memory. J Cogn Neurosci 2015;27(10):2019–2034.
26. Huang CC, Hsieh WJ, Lee PL, et al. Age-related changes in resting-state networks of a large sample size of healthy elderly. CNS Neurosci Ther 2015;21(10):817–825.
27. Farras-Permanyer L, Mancho-Fora N, Montalà-Flaquer M, et al. Age-related changes in resting-state functional connectivity in older adults. Neural Regen Res 2019;14(9):1544–1555.
28. Spreng RN, Turner GR. The Shifting Architecture of Cognition and Brain Function in Older Adulthood. Perspect Psychol Sci 2019;14(4):523–542.
29. Kelly AMC, Uddin LQ, Biswal BB, Castellanos FX, Milham MP. Competition between functional brain networks mediates behavioral variability. Neuroimage 2008;39(1):527–537.
30. Wang J, Liu J, Wang Z, Sun P, Li K, Liang P. Dysfunctional interactions between the default mode network and the dorsal attention network in subtypes of amnestic mild cognitive impairment. Aging (Albany NY) 2019;11(20):9147–9166.
31. Watanabe T, Sasaki Y, Shibata K, Kawato M. Advances in fMRI Real-Time Neurofeedback. Trends Cogn Sci 2017;21(12):997–1010 [Published correction appears in Trends Cogn Sci 2018;22(8):738.].